Image registration for Fizeau Fourier transform imaging spectroscopy

Samuel T. Thurman* and James R. Fienup
The Institute of Optics, University of Rochester, Rochester, New York 14627

ABSTRACT

Fourier transform imaging spectroscopy (FTIS) can be performed with a Fizeau imaging interferometer by recording a series of images with various optical path differences (OPDs) between subapertures of the optical system and post-processing. The quality of the spectral data is affected by misregistration of the raw image measurements. A Fizeau FTIS system possesses unique degrees of freedom that can be used to facilitate image registration without further complication of the system design. We describe a registration technique based on the fact that certain spatial frequencies of the raw imagery are independent of the OPDs introduced between subapertures. Operational and post-processing tradeoffs associated with this technique are described, and the technique is demonstrated using computer-simulated data with image shift misregistrations under realistic noise conditions.

Keywords: Fourier optics; digital image processing; phased-array imaging systems; telescopes; spectrometers and spectroscopic instrumentation

1. INTRODUCTION

In a Fizeau imaging interferometer, such as the multiple telescope array diagrammed in Fig.1, light collected by a number of relatively small subaperture telescopes is brought to focus via a set of beam combining optics [1]. Provided the optical path lengths through each subaperture are equal and certain design requirements are met [2], the system will operate as conventional imaging system having a pupil equal to the sum of the distributed subaperture pupil functions. Compared with a conventional optical system with pupil dimensions comparable to the dimensions of the distributed subapertures, a Fizeau interferometer can weigh significantly less and occupy a much smaller volume [3]. Tradeoffs include increased system complexity, reduced signal-to-noise ratio [4], and the need for image reconstruction algorithms [5].

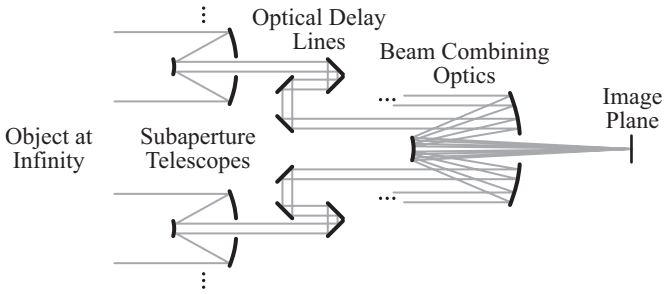

Figure 1. Fizeau imaging interferometer embodiment, a multiple-telescope array.

Typically a Fizeau imaging inteferometer has optical delay lines associated with each subaperture, which are used to minimize the optical path differences (OPDs) between subapertures for normal imaging. Alternatively, the delay lines can be used to introduce intentional OPDs between subapertures to perform Fourier transform imaging spectroscopy (FTIS) [6,7]. In this case, a sequence of panchromatic images is recorded for a series of OPDs and spectral data is obtained through the standard Fourier transform post-processing technique [8,9]. Similar FTIS can also be performed with a segmented-aperture telescope, using segment piston actuators to introduce the OPDs required for the spectroscopy. To put Fizeau FTIS in context, it can be compared to the baseline approach for performing Fourier transform spectroscopy with an imaging Michelson interferometer [10]. Compared with Michelson FTIS, the Fizeau system possesses unconventional imaging properties, which pose both technical challenges, namely the need for

* thurman@optics.rochester.edu; phone 1 585 275-8008; fax 1 585 244-4936

Algorithms and Technologies for Multispectral, Hyperspectral, and Ultraspectral Imagery XII,
edited by Sylvia S. Shen, Paul E. Lewis, Proc. of SPIE Vol. 6233,
62330S, (2006) · 0277-786X/06/$15 · doi: 10.1117/12.665593

nonlinear image reconstruction algorithms [11], and opportunities to develop novel operational and post-processing techniques that exploit these properties. An example of the later is the ability to dealias the spectral imagery obtained from a single set of aliased Fizeau FTIS measurements, without the need for micro-dithering [12]. Reference [9] contains a detailed analysis and discussion of the imaging properties of Fizeau FTIS.

In this paper, we discuss a novel approach to registering a set of Fizeau FTIS panchromatic intensity measurements. The registration technique is based on the imaging properties of Fizeau (or segmented optics) FTIS and, as such, is not applicable to Michelson FTIS systems. Registration of the panchromatic intensity measurements is vital to obtaining accurate spectral data from a FTIS system. Section 2 is a technical description of the technique. Section 3 discusses various operational and post-processing tradeoffs that facilitate the registration. Section 4 presents registration results from computer-simulated data with image-shift misregistrations. Section 5 draws conclusions.

2. REGISTRATION TECHNIQUE

Consider the case where an OPD = $c\tau$ is introduced between two groups of subapertures, where c is the speed of light and τ is a time-delay variable. We write the pupil function, $T(\xi,\eta,\nu,\tau)$, for such a system as

$$T\left(\xi,\eta,\nu,\tau\right)=T_1\left(\xi,\eta,\nu\right)+T_2\left(\xi,\eta,\nu\right)\exp\left(i2\pi\nu\tau\right), \tag{1}$$

where $T_1(\xi,\eta,\nu)$ and $T_2(\xi,\eta,\nu)$ are the pupil functions for the first and second groups of subapertures, respectively, (ξ,η) are pupil plane coordinates, and ν is optical frequency. The optical transfer function (OTF), $H(f_x,f_y,\nu,\tau)$, for such as system can be written as [13]

$$H\left(f_x,f_y,\nu,\tau\right)=\frac{T\left(-\lambda f_i f_x,-\lambda f_i f_y,\nu,\tau\right)\bigstar T\left(-\lambda f_i f_x,-\lambda f_i f_y,\nu,\tau\right)}{\int\limits_{-\infty}^{\infty}\int\limits_{-\infty}^{\infty}\left|T\left(\xi,\eta,\nu,\tau\right)\right|^2 d\xi d\eta}, \tag{2}$$

where λ is optical wavelength, f_i is the focal length of the imaging system, (f_x,f_y) are spatial-frequency coordinates, and $\bigstar$ is a two-dimensional cross-correlation operator with respect to the spatial-frequency coordinates.

As τ is varied, the panchromatic image varies because of the τ-dependency of the OTF, and hence the accurate registration of a collection of raw FTIS images is hampered by the corresponding changing point spread function (PSF). Defining $H_{p,q}(f_x,f_y,\nu)$ as the normalized cross-correlation between the p and q subaperture groups of the pupil function, *i.e.*,

$$H_{p,q}\left(f_x,f_y,\nu\right)=\frac{T_p\left(-\lambda f_i f_x,-\lambda f_i f_y,\nu\right)\bigstar T_q\left(-\lambda f_i f_x,-\lambda f_i f_y,\nu\right)}{\int\limits_{-\infty}^{\infty}\int\limits_{-\infty}^{\infty}\left|T\left(\xi,\eta,\nu,\tau\right)\right|^2 d\xi d\eta}, \tag{3}$$

the OTF can be written as

$$\begin{aligned}H\left(f_x,f_y,\nu,\tau\right)&=H_{1,1}\left(f_x,f_y,\nu\right)+H_{2,2}\left(f_x,f_y,\nu\right)\\&+H_{1,2}\left(f_x,f_y,\nu\right)\exp\left(-i2\pi\nu\tau\right)+H_{2,1}\left(f_x,f_y,\nu\right)\exp\left(i2\pi\nu\tau\right),\end{aligned} \tag{4}$$

using Eqs. (1) and (3). Written this way, it is plain to see that certain spatial frequencies are independent of τ, depending on the particular form of the subaperture pupil functions, *i.e.*, those passed by $H_{1,1}(f_x,f_y,\nu)$ and $H_{2,2}(f_x,f_y,\nu)$ only, while the remaining spatial frequencies passed by the optical system are dependent on τ. This fact makes it possible to accurately register a series of panchromatic intensity measurements made with different values of τ using the spatial frequencies that are independent of τ.

For the case of simple shift misregistrations, we use a weighted phase-only cross-correlation to accomplish the registration. Let $g(x,y,\tau)$ represent a series of raw FTIS image frames with spatial coordinates (x,y) recorded with different time delays τ, and suppose we wish to register the frames to a single frame, say $g(x,y,0)$. First, we define

$$f(x,y) = w(x,y)\, g(x,y,0), \tag{5}$$

where $w(x,y)$ is a window function used to mitigate edge effects by selecting a subregion of $g(x,y,0)$. Then the weighted phase-only cross-correlation between $f(x,y)$ and $g(x,y,\tau)$ is defined as

$$R_\phi(x,y) = \mathcal{F}^{-1}\left\{F_\phi(f_x,f_y)\, G_\phi^*(f_x,f_y,\tau)\, S(f_x,f_y)\right\}, \tag{6}$$

where $\mathcal{F}$ is a two-dimensional spatial Fourier transform operator, $S(f_x,f_y)$ is a Fourier-domain weighting function,

$$F_\phi(f_x,f_y) = \frac{\mathcal{F}\{f(x,y)\}}{\left|\mathcal{F}\{f(x,y)\}\right|}, \tag{7}$$

and

$$G_\phi(f_x,f_y,\tau) = \frac{\mathcal{F}\{g(x,y,\tau)\}}{\left|\mathcal{F}\{g(x,y,\tau)\}\right|}. \tag{8}$$

The x and y shift misregistrations are determined by finding the location of the maximum of $R_\phi(x,y)$. Based on the imaging properties of Fizeau FTIS, we propose a choice of $S(f_x,f_y)$ that emphasizes spatial frequencies that are independent of τ, *i.e.*, those passed by $H_{1,1}(f_x,f_y,\nu)$ and $H_{2,2}(f_x,f_y,\nu)$ only. The particular form of $S_k(f_x,f_y)$ is discussed in Sec. 3.

In contrast to Fizeau FTIS, the beamsplitter in an imaging Michelson interferometer effectively divides the complete pupil of the optical system into two identical pupil functions, *i.e.*, $T_1(\xi,\eta,\nu) = T_2(\xi,\eta,\nu)$. Thus, all of the $H_{p,q}(f_x,f_y,\nu)$ terms are identical, which implies that all of the spatial frequencies (f_x,f_y) passed by the optical system are dependent on τ. So the method that we propose for registering the raw Fizeau FTIS frames is not applicable to Michelson FTIS. One approach for helping to register Michelson FTIS frames is to use a four-port interferometer design, which requires two detector arrays. In such a system, the sum of the image intensities at both detectors is independent of the OPD between the arms of the interferometer.

3. OPERATIONAL AND POST-PROCESSING TRADEOFFS

For accurate registration using the method that we propose, the raw Fizeau FTIS imagery should ideally possess high spatial-frequency components that are independent of τ in at least two nearly-orthogonal directions. While the forms of $H_{1,1}(f_x,f_y,\nu)$ and $H_{2,2}(f_x,f_y,\nu)$ are important for registration of the raw intensity measurements, the terms $H_{1,2}(f_x,f_y,\nu)$ and $H_{2,1}(f_x,f_y,\nu)$ are of primary interest for FTIS since they are the imaging transfer functions for the resulting spectral imagery [9]. For a given system, the division of subapertures into groups $T_1(\xi,\eta,\nu)$ and $T_2(\xi,\eta,\nu)$ for FTIS operation is a tradeoff that can be used to help achieve $H_{p,q}(f_x,f_y,\nu)$ terms that are favorable for both registration and spectral imaging. As an example, Fig. 2 shows various choices of $T_1(\xi,\eta,\nu)$ and $T_2(\xi,\eta,\nu)$ for a multiple-telescope array with six subapertures, and the resulting $H_{p,q}(f_x,f_y,\nu)$ terms. For the subaperture grouping indicated by Fig. 2(a), notice that there are high spatial frequencies passed only by $H_{1,1}(f_x,f_y,\nu)$ and $H_{2,2}(f_x,f_y,\nu)$ in a single direction (30° counterclockwise from the vertical axis). Thus, the registration technique is likely to determine image shifts along this direction well, but is not expected to work as well for image shifts in the orthogonal direction. Additionally, the $H_{1,2}(f_x,f_y,\nu)$ and $H_{2,1}(f_x,f_y,\nu)$ terms are zero along this direction, which means that the resulting spectral imagery will be missing spatial frequencies in this direction. For the subaperture grouping of Fig. 2(f), there are high spatial frequencies passed only by $H_{1,1}(f_x,f_y,\nu)$ and $H_{2,2}(f_x,f_y,\nu)$ in two directions (0° and 60° counterclockwise from the vertical axis). For the subaperture

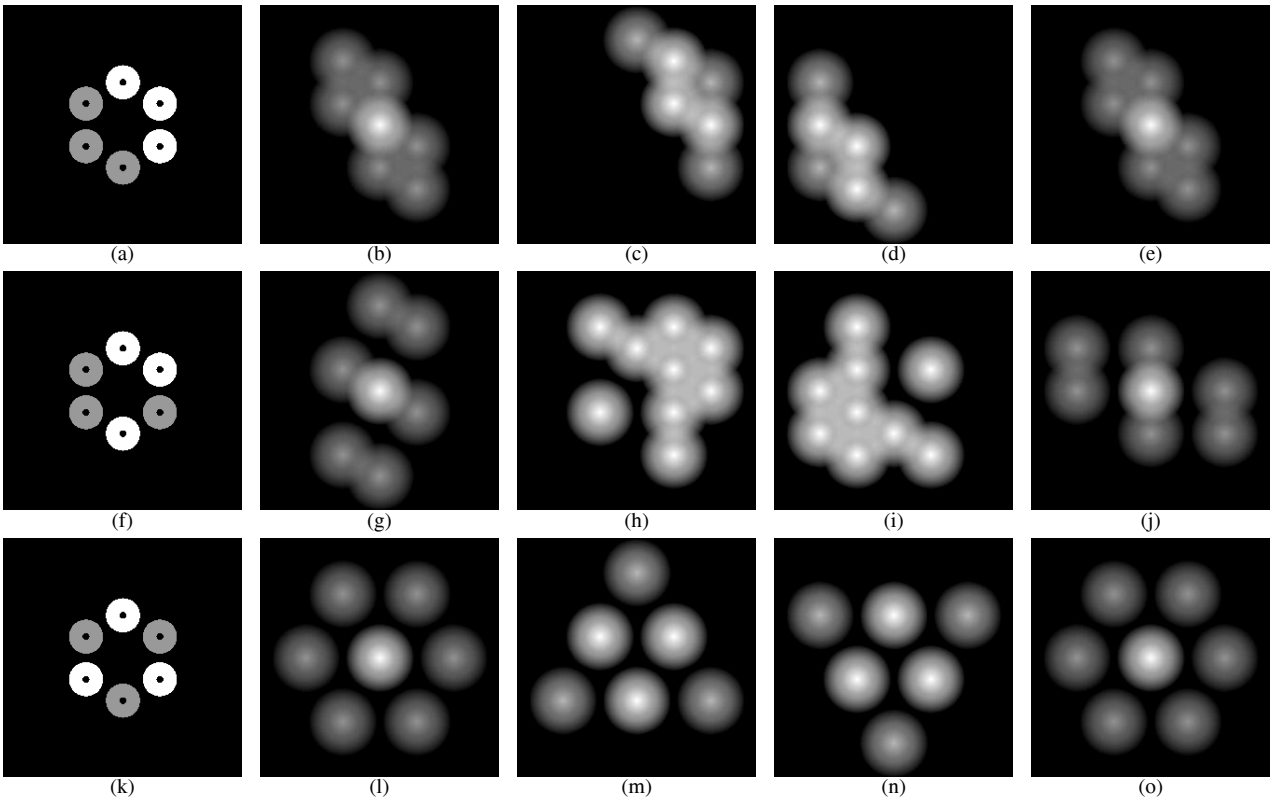

Figure 2. OTF terms for different choices of $T_1(\xi,\eta,\nu)$ and $T_2(\xi,\eta,\nu)$ for a multiple-telescope array with six subapertures: the first column shows the pupil of the system where $T_1(\xi,\eta,\nu)$ is indicated by white and $T_2(\xi,\eta,\nu)$ is indicated by gray, the remaining columns show the resulting $H_{1,1}(f_x,f_y,\nu)$, $H_{1,2}(f_x,f_y,\nu)$, $H_{2,1}(f_x,f_y,\nu)$, and $H_{2,2}(f_x,f_y,\nu)$ terms (for a single ν), respectively, where each row corresponds to a different choice of $T_1(\xi,\eta,\nu)$ and $T_2(\xi,\eta,\nu)$.

grouping of Fig. 2(k), there are high spatial frequencies passed only by $H_{1,1}(f_x,f_y,\nu)$ and $H_{2,2}(f_x,f_y,\nu)$ in *three* directions (30°, 90°, and 120° counterclockwise from the vertical axis). Thus, the grouping of Fig. 2(k) is preferable from the standpoint of the number of directions along which there are high spatial frequencies independent of τ. Also, the forms of $H_{1,2}(f_x,f_y,\nu)$ and $H_{2,1}(f_x,f_y,\nu)$ for both of these groupings are favorable for spectral imaging in that they yield spectral imagery with spatial-frequency content in all directions. Note that any other grouping of the subapertures into two groups of three subapertures is equivalent to one of the cases shown in Fig. 2 through a rotation and/or a reflection.

Additionally, there are post-processing tradeoffs associated with the particular choice of the weighting function $S(f_x,f_y)$. Consider binary weighting functions of the form

$$S_\kappa\left(f_x,f_y\right)=\begin{cases}1 & \text{for } \left|\bar{H}_{1,1}\left(f_x,f_y\right)\right|+\left|\bar{H}_{2,2}\left(f_x,f_y\right)\right|>\kappa\left|\bar{H}_{1,2}\left(f_x,f_y\right)\right|+\kappa\left|\bar{H}_{2,1}\left(f_x,f_y\right)\right| \\ 0 & \text{otherwise,}\end{cases} \tag{9}$$

where κ is a parameter, and $\bar{H}_{p,q}(f_x,f_y)$ represents a spectral average of $H_{p,q}(f_x,f_y,\nu)$ over the spectral bandwidth of the imagery. Figure 3 shows $S_\kappa(f_x,f_y)$ for the system and subaperture grouping of Fig. 2(k) for several values of κ, along with plots of $s_\kappa(x,y)$, the inverse Fourier transform of $S_\kappa(f_x,f_y)$. For $S_{100}(f_x,f_y)$, shown in Fig. 3(a), $R_\phi(x,y)$ essentially includes only spatial-frequency components that are independent of τ, but $s_{100}(x,y)$ has large sidelobes, which can lead to problems in the registration of noisy imagery. To understand this, note that $R_\phi(x,y)$ [see Eq. (6)] will essentially be a shifted version of $s_\kappa(x,y)$ in the absence of noise [ignoring effects of the window function, $w(x,y)$]. Since the sidelobes

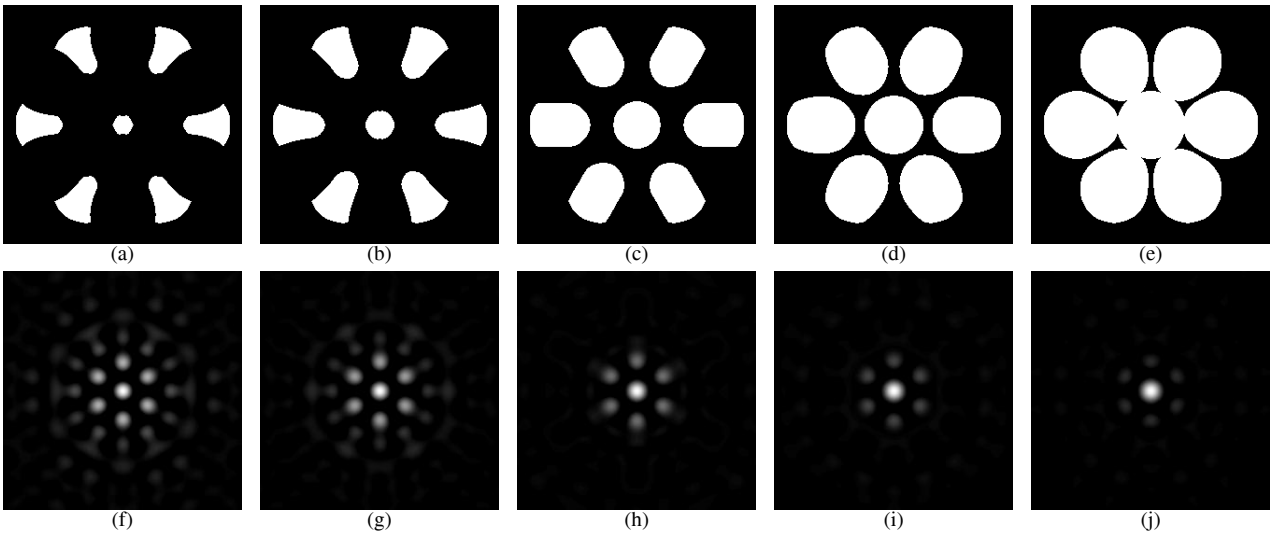

Figure 3. Post-processing tradeoffs associated with choosing $S(f_x,f_y)$ for the system and subaperture grouping of Fig. 2(k) for a spectral bandwidth λ = 2.0–2.5 μm: the top row shows $S_\kappa(f_x,f_y)$ for (a) κ = 100, (b) κ = 10, (c) κ = 1, (d) κ = 0.1, and (e) κ = 0, while the bottom row shows the corresponding $s_\kappa(x,y)$ (zoomed in, upsampled by 10x, and negative values clipped).

of $R_\phi(x,y)$ are relatively large compared to the central peak, it is conceivable that any one of the sidelobes could be greater than the central peak in the presence of noise, leading to an inaccurate registration. One way to avoid this is to decrease κ, which has the effects of broadening $S_\kappa(f_x,f_y)$ and reducing the sidelobes of $s_\kappa(x,y)$, as shown in Fig. 3. An additional benefit of reducing κ is that the signal-to-noise ratio of $R_\phi(x,y)$ is increased, since the number of data points used in the calculation of $R_\phi(x,y)$ is increased. On the other hand, decreasing κ causes spatial frequencies that are dependent on τ to be included in $R_\phi(x,y)$, which works against our original strategy for choosing $S(f_x,f_y)$. Thus, there is a post-processing tradeoff associated with the choice of the value for κ: too large of a value increases noise susceptibility, while too small of a value increases the number of τ-dependent spatial frequencies in the calculation of $R_\phi(x,y)$, both of which can lead to inaccurate registrations. The simulation results in Sec. 4 demonstrate this tradeoff.

4. SIMULATION RESULTS

We performed a computer simulation to demonstrate the registration technique. The object data was taken from AVIRIS [14] (data set: f970619t01p02_r02), trimmed spatially to 512×512 samples and spectrally to λ = 1.93–2.50 μm. This data was used as the object radiance as seen from the entrance pupil of the optical system. The optical system was an array of six telescopes arranged in ring as shown in Fig. 2. Tables 1 and 2 list various parameters and their values for the simulation. For simulating Fizeau FTIS, the subaperture telescopes were grouped as indicated by Fig. 2(f). A sequence of 256 image frames were simulated for the range of τ = –384 to 381 fs with a uniform sample spacing of $\Delta\tau$ = 3.00 fs (the corresponding OPD range is –115 to 114 μm and OPD sample spacing is 0.900 μm). Shift misregistrations and edge effects were included in each frame as follows: (i) calculating a noiseless 512×512 image, (ii) shifting each image via a linear phase function in the spatial-frequency domain, and (iii) cropping each image to 480×480 pixels. The standard deviation of the misregistrations in the x and y directions was 8 pixels. Figure 4 shows the actual misregistrations used in the simulation as a function of τ. Note that the misregistration between frames are correlated to resemble a pointing error that is slowly varying compared to the exposure time. After introducing the misregistrations, photon and read noise were added and the images were converted to digital number units. The average signal level was 2.74×10^4 e^-, yielding an average signal-to-noise ratio for the raw intensity measurements of 158, due to photon and read noise. Figure 5 shows the object and two image frames from the simulation. Note that while Fig. 5(c) appears less sharp than Fig. 5(b) due to the τ difference between the subaperture groups, there are certain high spatial-frequency features, (those which are independent of τ) that are the same.

Table 1. Optical system parameters used for simulation.

Parameter	Value
Diameter of individual subaperture	0.40 m
Diameter of central obscurations	0.08 m
Encircled diameter of array	1.40 m
F-number of array	30
Optical efficiency (transmission)*	50%
Spectral bandwidth	λ = 1.93–2.50 μm

*Assumed to be uniform over the spectral bandwidth of the simulation.

Table 2. Detector parameters used for simulation.

Parameter	Value
Pixel pitch	28 μm
Quantum efficiency†	65%
Fill factor	90%
Well depth	40,000 e^-
Read noise standard deviation	50e^-
A/D converter bits	12
A/D converter gain	10 e^-/DN
Exposure time	10 ms

†Assumed to be uniform over the spectral bandwidth of the simulation.

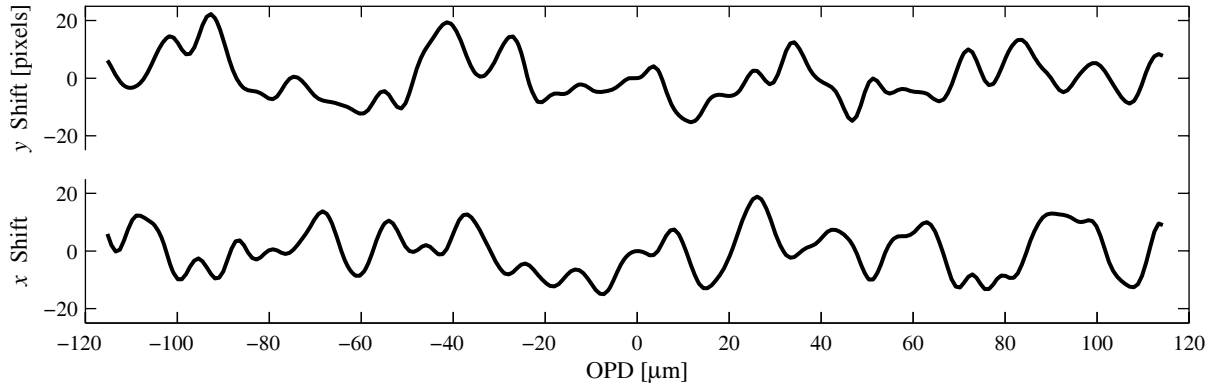

Figure 4. Shift misregistrations included in the simulation plotted as a function of the OPD between the subaperture groups for each frame of the raw Fizeau FTIS intensity measurements.

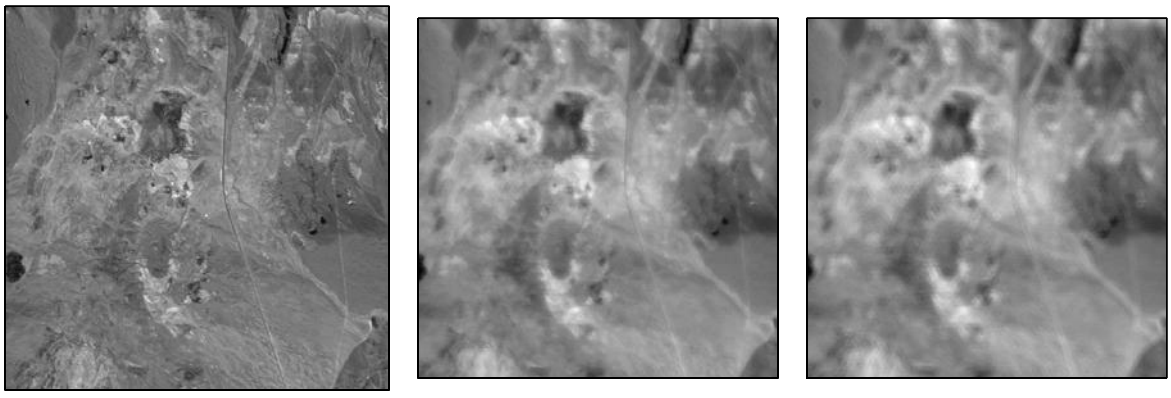

(a) (b) (c)

Figure 5. Simulation data: (a) panchromatic view of the object, and image frames for (b) τ = 0 fs (OPD = 0 μm) and (c) τ = 3.00 fs (OPD = 0.900 μm), where each image is linearly stretched and (b) and (c) are smaller than (a) due to cropping.

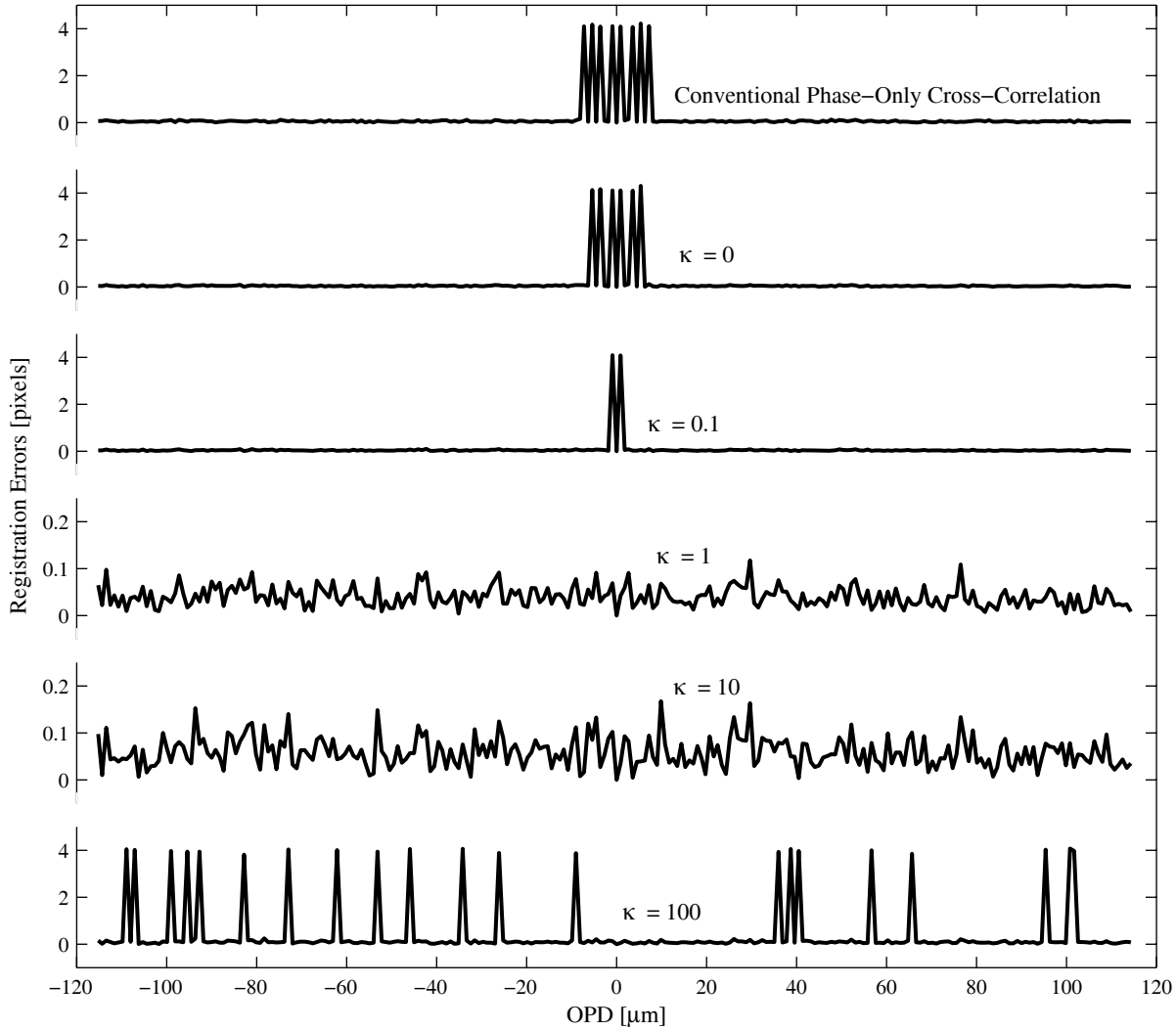

Figure 6. Registration errors plotted vs. OPD between the subaperture groups for various choices of $S(f_x,f_y)$: a conventional phase-only cross correlation, where $S(f_x,f_y) = 1$ for all (f_x,f_y) within the support of the OTF and $S(f_x,f_y) = 0$ otherwise, and $S_\kappa(f_x,f_y)$ for $\kappa = 0$, 0.1, 1, 10, and 100.

The raw intensity measurements were registered using various choices of $S(f_x,f_y)$. In each case, the $\tau = 0$ image frame was used as the master frame (to which all of the other image frames were registered), and a square window with raised-cosine tapered edges was used for $w(x,y)$. For comparison, the frames were registered using a conventional phase-only cross-correlation, where $S(f_x,f_y) = 1$ for all (f_x,f_y) within the support of the OTF (averaged over the spectral bandwidth of the simulation) and $S(f_x,f_y) = 0$ otherwise. Additionally, the frames were registered using $S_\kappa(f_x,f_y)$ defined in Eq. (9) for $\kappa = 0$, 0.1, 1, 10, and 100. In each case, the peak of $R_\phi(x,y)$ was determined initially as the maximum of a 2x upsampled version of $R_\phi(x,y)$ and then refined using a nonlinear optimization routine. Figure 6 shows the registration errors for the various choices of $S(f_x,f_y)$. The registration error is the magnitude of the orthogonal errors in the x- and y-directions. Most of the registration errors are considerably less than one pixel, while there are several outliers with registration errors of about 4 pixels. Figure 7 is a scatter plot of the x and y registration errors for all choices of $S(f_x,f_y)$. Notice that all of the outliers are arranged in a hexagonal pattern identical to the sidelobe features for $s_\kappa(x,y)$ shown in the bottom row of Fig. 3. Noise can cause registration outliers by making one of the sidelobes of $R_\phi(x,y)$ become larger

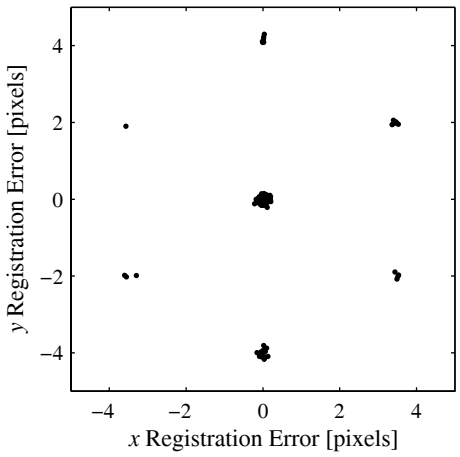

Figure 7. Scatter plot of registration errors for all choices of $S(f_x,f_y)$.

Table 3. Registration results for simulation.

$S(f_x,f_y)$	Number of Outliers‡	RMS Registration Error [pixels]	
		Outliers Included	Outliers Excluded
Conventional phase only	8	0.710	0.028
$\kappa = 0$	6	0.623	0.021
$\kappa = 0.1$	2	0.358	0.019
$\kappa = 1$	0	0.021	0.021
$\kappa = 10$	0	0.031	0.031
$\kappa = 100$	21	1.070	0.044

‡Where outliers is defined as a registration error greater than one pixel.

than the central peak. Also, the inclusion of τ-dependent spatial frequencies in $S(f_x,f_y)$ can cause outliers due to the modulation of certain spatial frequencies with respect to τ. While this has a somewhat complicated effect on the peak and sidelobes of $R_{\phi\phi}(f_x,f_y)$, it leads to misregistration outliers belonging to the same hexagonal pattern due to the hexagonal symmetry of the subaperture arrangement and grouping. While the probability of an outlier occurring due to noise is independent of τ, the likelihood of an outlier occurring due to the inclusion of τ-dependent spatial frequencies is highest near $\tau = 0$, or OPD = 0, where the visibility of the modulation is greatest. Having said this, the registration errors shown in Fig. 6 indicate that the conventional phase-only weighting function $S(f_x,f_y)$ and $S_\kappa(f_x,f_y)$ for $\kappa \leq 0.1$ are susceptible to registration outliers due to the inclusion of τ-dependent spatial frequencies, while $S_\kappa(f_x,f_y)$ for $\kappa \geq 100$ is prone to registration outliers due to noise. Between these extremes, for $S_\kappa(f_x,f_y)$ for $\kappa \approx 1$–10, the probability of registration outliers occurring is minimized. Table 3 is a numerical summary of the registration results obtained with the various choices of $S(f_x,f_y)$.

5. CONCLUSIONS

The unique imaging properties of Fizeau FTIS provide opportunity for operational and post-processing techniques not applicable to Michelson FTIS. Registration of the panchromatic intensity measurements is an example of this. We have described a registration technique based on the principle that certain spatial frequencies are independent of the OPDs introduced for performing Fizeau FTIS. We have described operational and post-processing tradeoffs associated with this technique and demonstrated through computer simulation that the technique can yield accurate registrations under realistic conditions. While this demonstration only considered misregistrations due to image shift, the registration principle is generally applicable to other types of misregistration, *e.g.*, rotation, scale, and keystone.

6. ACKNOWLEDGEMENT

This work was supported by Lockheed Martin Corporation.

7. REFERENCES

1. A. B. Meinel, "Aperture synthesis using independent telescopes," Appl. Opt. **9**, 2501-2504 (1970).
2. L. D. Weaver, J. S. Fender, and C. R. De Hainaut, "Design considerations for multiple telescope imaging arrays," Opt. Eng. **27**, 730-735 (1988).
3. J. S. Fender, "Synthetic apertures: an overview," in *Synthetic Aperture Systems*, J. S. Fender, ed., Proc. SPIE **440**, 2-7 (1983).
4. J. R. Fienup, "MTF and integration time versus fill factor for sparse-aperture imaging systems," in *Imaging Technologies and Telescopes*, J. W. Bilbro, *et al.*, eds., Proc. SPIE **4091**, 43-47 (2000).
5. J. R. Fienup, D. Griffith, L. Harrington, A. M. Kowalczyk, J. J. Miller, and J. A. Mooney, "Comparison of reconstruction algorithms for images from sparse-aperture systems," in *Image Reconstruction from Incomplete Data II*, P. J. Bones, *et al.*, eds., Proc. SPIE **4792**, 1-8 (2002).
6. M. Frayman and J. A. Jamieson, "Scene imaging and spectroscopy using a spatial spectral interferometer," in *Amplitude and Intensity Spatial Interferometry*, J. B. Breckingridge, ed., Proc. SPIE **1237**, 585-603 (1990).
7. R. L. Kendrick, E. H. Smith, and A. L. Duncan, "Imaging Fourier transform spectrometry with a Fizeau interferometer," in *Interferometry in Space*, M. Shao, ed., Proc. SPIE **4852**, 657-662 (2003).
8. J. Kauppinen and J. Partanen, *Fourier Transforms in Spectroscopy*, (Wiley-VCH, Berlin, 2001).
9. S. Thurman and J. Fienup, "Multi-aperture Fourier transform imaging spectroscopy: theory and imaging properties," Opt. Express **13**, 2160-2175 (2005), http://www.opticsexpress.org/abstract.cfm?URI=OPEX-13-6-2160.
10. N. J. E. Johnson, "Spectral imaging with the Michelson interferometer," in *Infrared Imaging Systems Technology*, Proc. SPIE **226**, 2-9 (1980).
11. S. T. Thurman and J. R. Fienup, "Fizeau Fourier transform imaging spectroscopy: direct nonlinear image reconstruction" (submitted to Optics Express).
12. S. T. Thurman and J. R. Fienup, "Dealiased spectral images from aliased Fizeau Fourier transform imaging spectroscopy measurements," in Frontiers in Optics 2005/Laser Science XXI (Optical Society of America, Washington, DC, 2005), paper FTuM2.
13. J. Goodman, *Introduction to Fourier Optics 3rd ed.*, (Roberts & Co., Greenwood Village, Colorado, 2004).
14. Provided through the courtesy of Jet Propulsion Laboratory, California Institute of Technology, Pasadena, California, http://aviris.jpl.nasa.gov/.